

Article

Design of Valve Seating Buffer for Electromagnetic Variable Valve System

Qingya Zhou, Liang Liu ^{*}, Cong Zheng, Zhaoping Xu  and Xianhui Wang

School of Mechanical Engineering, Nanjing University of Science and Technology, Nanjing 210014, China

^{*} Correspondence: l.liu@njust.edu.cn

Abstract: An electromagnetic variable valve (EMVV) system can significantly reduce pumping loss and discharge loss of the engine by enabling variable valve timing and variable valve lift. However, the valve seat easily produces a larger impact collision with the engine cylinder head because of fast valve seating velocity, greatly decreasing engine life. Therefore, in this paper, a valve seating buffer (VSB) is designed to solve the problem of large electromagnetic valve seating impact. Firstly, a scheme of an EMVV system with embedded buffer is proposed, the collision model is established to resolve the problem of the soft landing of the valve and the effectiveness of the model is verified by experiment. In addition, the structure, material and dimension parameters of the proposed buffer are designed, and some key parameters of the buffer are optimized by the Nelder–Mead (N–M) algorithm. Finally, a co-simulation model of the actuator and the buffer is built, and the valve seating performance is analyzed. The co-simulation results show that the valve seating velocity and rebound height of the EMVV system with the designed buffer are reduced by 94.8% and 97%, respectively, which verifies the advantages of the designed VSB.

Keywords: electromagnetic variable valve; seating buffer; soft landing; design and optimization



Citation: Zhou, Q.; Liu, L.; Zheng, C.; Xu, Z.; Wang, X. Design of Valve Seating Buffer for Electromagnetic Variable Valve System. *Actuators* **2023**, *12*, 19. <https://doi.org/10.3390/act12010019>

Academic Editor: Ioan Ursu

Received: 30 November 2022

Revised: 28 December 2022

Accepted: 30 December 2022

Published: 1 January 2023



Copyright: © 2023 by the authors. Licensee MDPI, Basel, Switzerland. This article is an open access article distributed under the terms and conditions of the Creative Commons Attribution (CC BY) license (<https://creativecommons.org/licenses/by/4.0/>).

1. Introduction

Due to the rapid development of new energy vehicles, improving the performance of traditional internal combustion engine vehicles can greatly ease the competition within the automotive industry and the crisis of energy form change. Variable valve trains significantly reduce pumping loss and discharge loss of engine by enabling a continuously variable phase and lifting of the valve. At present, a variable valve train mainly includes either an electro-hydraulic drive, electric drive or an electromagnetic drive [1]. Compared with the first two, the electromagnetic variable valve (EMVV) system does not need a transfer medium, and it has a simple structure and high power density. There have been many related research cases in the world, and it has become a research hotspot in related fields [2,3]. Although an EMVV system can realize the continuous adjustment and movement of the valve opening and closing, the external force easily interferes with valve opening and closing because of its structural characteristics, and the control accuracy is also affected. In addition, due to the fast velocity of the valve seating, it is easy to have a large impact collision with the engine cylinder head, and it can produce a large noise; it also has a greater impact on the engine life. Therefore, the scheme of the valve seating buffer (VSB) is extremely important for an EMVV system.

Currently, the scheme of the VSB of an electromagnetic drive valve train mainly includes control strategy research and an external mechanism. Yang et al. [4] designed an energy compensation control for an optimized engine electromagnetic valve; valve “zero” seating velocity was achieved by neutralizing positive and negative work in the armature stroke. Paden et al. [5] proposed a new type of EMVV structure, and the rapid response of the valve between opening and closing state was realized through the implementation of a control strategy while ensuring low valve seating velocity and power consumption.

Compared to traditional, complex control strategies, the method of using external buffers has lower difficulty and does not require study of sophisticated control strategies; it can achieve valve seat buffering in the most simple and reliable way. Tu et al. [6] used a one-way throttle valve to buffer the electro-hydraulic drive valve mechanism; the best buffer effect was achieved by changing throttling area and throttling stroke of the throttle valve, and the seating velocity was reduced, and the dynamic response of the valve was improved in this way. Pan et al. [7] added a one-way valve to the upper end of the valve plunger to buffer the valve seating; the valve was simultaneously subjected to the oil pressure and spring force of the valve system during seating, which effectively decreased the valve seating velocity. Xu et al. [8] introduced the disc spring into the EMVV system, so that it acted between the valve and the coil, which could store most of the kinetic energy of the coil and effectively reduced the impact stress by about 50%. The faster the seating velocity, the more obvious the effect. Nowadays, most of the solutions for valve seating buffer are realized by control methods, but, because the valve seating is fast, and the time is short, the control is really a difficult method.

Buffering, as an important part of shock absorption, is often used in vehicles, bridges, aerospace and other fields. Magnetorheological buffers have attracted much attention in recent years due to their low energy consumption, fast response and large output damping force. The working principle of magnetorheological fluid is to control the magnetic induction intensity in the flow channel by adjusting the current intensity of the coil and then changing the shear yield strength of the magnetorheological fluid, affecting the pressure drop at both ends of the buffer flow channel so as to achieve the purpose of outputting the buffer force. It has the advantages of stable performance, low input voltage and large yield stress. David Case et al. [9] designed a small magnetorheological buffer for upper limb orthosis and model building, and experimental verification of the buffer was carried out, and the feasibility of applying small magnetorheological buffer to tremor motion attenuation was discussed. T.M. Gurubasavaraju et al. [10] proposed a scheme applying a magnetorheological buffer to a semi-active suspension system; a quarter of the vehicle models were analyzed under different road conditions. The results showed that the semi-active suspension with magnetorheological buffer had better regularity and road stability. Alan Sternberg et al. [11] proposed a large magnetorheological buffer for reducing the vibration of high-rise buildings; the design, manufacture and testing of the buffer prototype were completed. The test results were in good agreement with the established finite element model. In the actual design of magnetorheological buffers, most researchers often obtain some key parameters through experience, such as the size of the flow channel gap, the piston, etc. Therefore, it is necessary to optimize the structural parameters of the magnetorheological buffer after the structural design. Mao et al. [12] proposed an optimistic method of the structuring of a magnetorheological buffer by using a nonlinear flow model; the test showed that the performance of the optimized prototype was greatly improved. Guan et al. [13] used a multi-objective genetic algorithm, selected the output buffer force and adjustable multiple of the buffer as the optimization objectives, optimized the seven key variables of the magnetorheological buffer and, finally, obtained a large buffer force and highly adjustable multiple. Wu et al. [14] optimized the magnetic circuit of a magnetorheological buffer through the APDL parametric language built-in ANSYS and achieved the expected requirements. Yang et al. [15] proposed a novel structure of the annular multi-channel magnetorheological valve, designed its magnetic circuit and improved the pressure drop performance of the annular multi-channel magnetorheological valve.

In this paper, a scheme for adding a VSB is proposed to solve the problem of the large seating impact of electromagnetic valve, and the VSB is designed and optimized. An EMVV can effectively improve the power and fuel economy of an engine, but the existing integration layout of the system cannot meet the problem of limited setting space during actual installation, and the traditional modeling method cannot fully show the complex coupling structural characteristics of the EMVV system. Therefore, this paper firstly proposes a new structure for an EMVV system and then a collision model is established

for the problem of soft landing, and the model is verified by Zheng's [16] test bench. The structure, material and size parameters of the proposed buffer are designed in detail, and some key parameters of the buffer are optimized by the Nelder–Mead (N-M) algorithm. Finally, a co-simulation model is built based on the coupling relationship between the actuator and the buffer of the EMVV system; the effectiveness and advantages of the designed VSB are verified by analyzing the valve seating performance of the system.

2. System Scheme

2.1. Overall Scheme

The structure of EMVV system, shown in Figure 1, mainly includes EMVA, VSB and valve components. The EMVA is the component that drives the valve opening and closing, and the performance of the EMVA determines whether the system can achieve rapid opening and closing. The valve seating buffer (VSB) is the component that reduces the valve seating velocity when the valve is seated. It needs to be able to output a larger buffer force and a faster response speed, so that it can reduce the velocity in a very short time and achieve valve seat buffering. The working principal of the EMVV system is: when the valve is opening, the coil of the actuator is activated. The coil is driven by the axial electromagnetic force and moves in the magnet field generated by the permanent magnet; thus, the valve is controlled to open. Continuously adjustable valve lift and transition time can be achieved by controlling the current of the coil. When the valve is seated, the coil of the buffer is soon activated. The buffer produces a controllable buffer force opposite to the direction of motion of the valve, thus, realizing the deceleration and the soft landing of the valve. In Figure 1, the VSB designed in this paper is shown; it consists of a magnetorheological fluid, piston, cylinder and coil, etc.

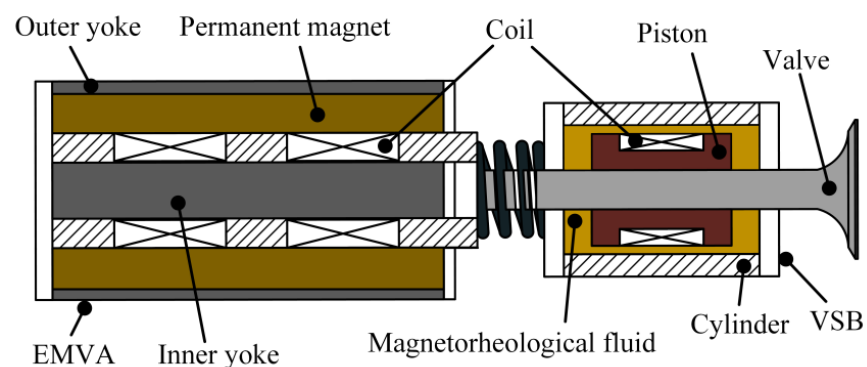


Figure 1. The structure of EMVV system.

2.2. System Design Scheme

Zheng et al. [16] proposed a parallel structure of EMVV, as shown in Figure 1. The scheme has a larger deficiency. On the one hand, the maximum buffer force that the buffer can output is 35 N, which cannot meet the needs of valve seating. On the other hand, the scheme needs greater setting space and aggravates the engine burden. Therefore, a new scheme is proposed in this paper, as shown in Figure 2. As the core components of the whole system, the actuator and the buffer adopt an integrated layout scheme. The buffer is placed in the hole pulled out by the inner yoke of the actuator. The piston rod is connected with the coil of the actuator and the valve components. The scheme greatly reduces the volume of the whole system, which is a tremendous boost for the engine in its limited setting space.

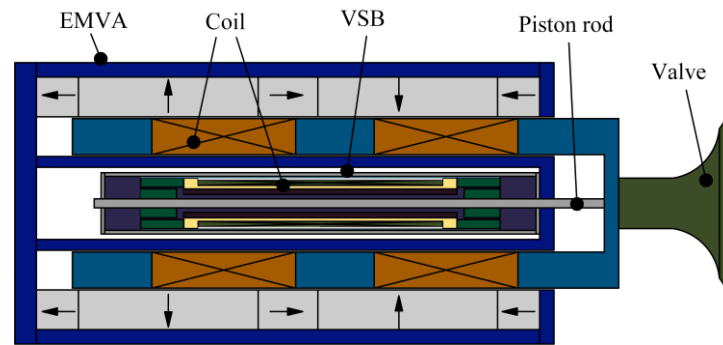


Figure 2. New structure of EMVV system.

2.3. System Modeling

2.3.1. Collision Modeling

The coil of the EMVA is driven by electromagnetic force. When the coil moves to the upper and lower ends of the stroke, it collides with the upper and lower yokes and produces a rebound. This phenomenon causes the valve to have a greater impact and noise on the engine cylinder head during valve seating and affects the engine life. In order to establish a complete simulation model with collision module of the system, it is necessary to identify the collision parameters between the coil skeleton and the yoke. According to collision theory [17], when two objects collide, the stiffness coefficient and damping coefficient are the main parameters affecting collision velocity and rebound height. The specific collision model is shown in Figure 3. The combination of spring and damper can be used to represent the collision model of the coil skeleton and yoke during collision. Among them, R represents that the slider moves in the track X with upper and lower boundaries. K_p and K_n represent the contact stiffness coefficients of the upper and lower boundaries, respectively. D_p and D_n represent the damping coefficients of the upper and lower boundaries, respectively. G_p and G_n represent the distances from the slider to the upper and lower boundaries. The coil stroke in the actuator is $(G_p + G_n)$.

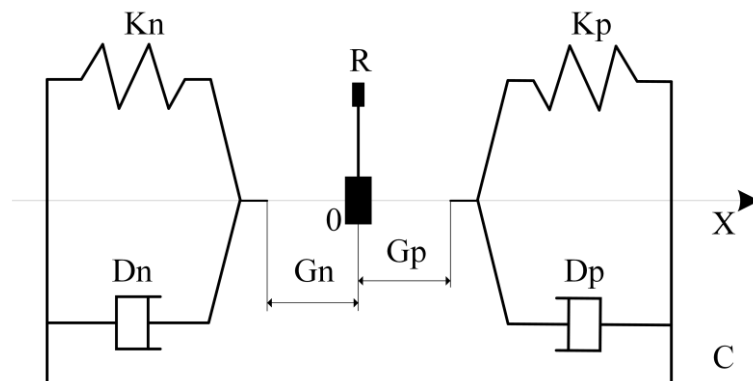


Figure 3. Collision model.

Based on the collision model, the stiffness coefficient and damping coefficient are used to establish the rebound module in the multi-physics finite element model of the system. In this paper, the recursive least-squares method is used to identify the collision parameters between the coil and the yoke. Compared to the traditional least-squares method, the inversion accuracy of the matrix in the recursive least-squares method does not affect the final identification results, and it can predict and update the data, significantly reducing computation. The main steps of collision parameter identification are as follows:

1. Analyze the dynamic principle during coil collision with yoke and establish the dynamic equation and finite element model of collision;

2. Build datasets of the stiffness coefficient and damping coefficient according to the calculation results of the dynamic equation;
3. Run 10 groups of different parameter combinations on the established, transient finite element model and collect velocity and rebound height and average them;
4. Compare the processed velocity and bounce height with test results to verify the correctness of the parameters;
5. Check whether the theoretical collision velocity and rebound height match the test; if not, check whether the finite element model and parameter equation are correct and identify again until the results meet the requirements.

According to the above steps, the stiffness coefficient is 5×10^7 N/m, and the damping coefficient is 1000 N·s/m. The finite element modeling of EMVA is carried out by using the identified collision parameters.

2.3.2. Model Simulation and Verification

Based on the above collision model, a sinusoidal current with an amplitude of 10 A and a frequency of 20 Hz is applied to the actuator. The motion state of the actuator coil is shown in Figure 4. As can be seen from the figure, the coil originally in the center of the air gap begins to move upwards under the action of electromagnetic force and collides with the upper yoke. The velocity at contact is 1.97 m/s, and the rebound height is 0.4 mm. Half a cycle later, the direction of the electromagnetic force becomes downward, and the coil moves downward (a stroke is 8 mm) and collides with the lower yoke; the collision velocity is 3.3 m/s, and the rebound height is 0.66 mm.

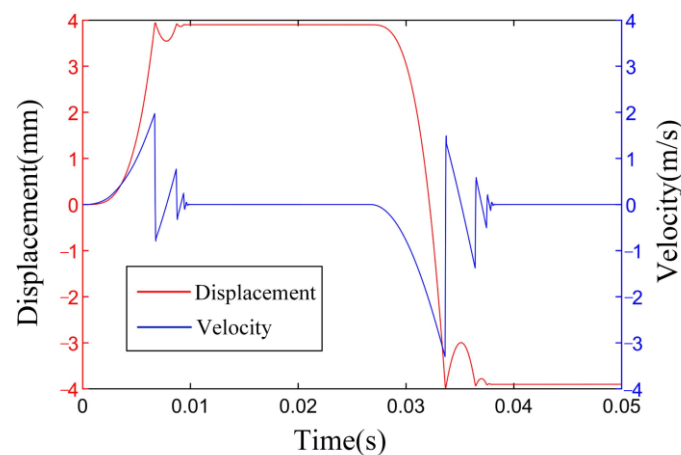


Figure 4. Displacement and velocity curves of coil.

The simulation model and the test bench of the valve seating buffer build by Zheng et al. [16] are used to verify the effectiveness of the collision model. The valve seating test of the EMVV system is carried out according to the established control strategy; the buffer is closed. The comparison results of simulation and experiment are shown in Figure 5; when the valve lift is 8 mm, the valve seating velocity is 0.71 m/s and 0.58 m/s, and the rebound height is 0.7 mm and 0.25 mm, respectively. The experiment verifies the effectiveness of the established collision model by simulating the impact on the cylinder head of the engine when the valve is quickly seated. Tests have found that reducing the impact can greatly reduce mechanical noise and extend the engine life. Therefore, the valve seating buffer is very important.

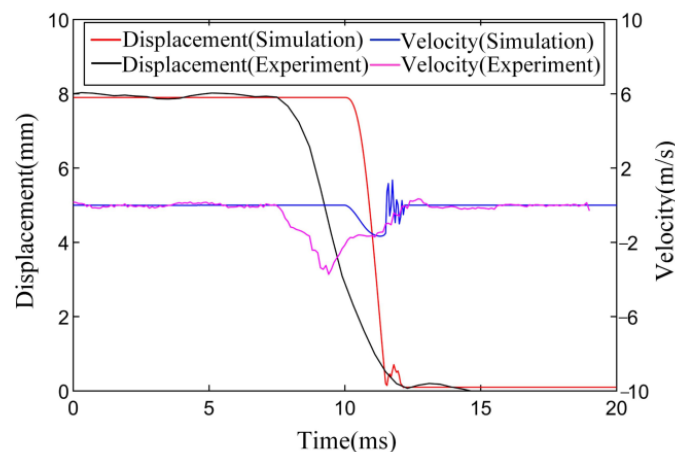


Figure 5. Comparison curves of the valve between experiment and simulation.

3. Design of Valve Seating Buffer

3.1. Structure Design

The magnetorheological buffer consists of a piston, piston rod, cylinder, cover, coil and magnetorheological fluid. When the buffer works, the piston rod drives the piston to move, the magnetorheological fluid with increased viscosity under the action of the magnetic field generated by the coil is squeezed, forms pressure difference and generates buffer force. In general, the magnetorheological buffer can be divided into a damping unit and a damping cylinder.

3.1.1. Channel Form

The flow channel of the damping unit is a channel that, through the magnetorheological fluid, affects the output buffer force. The main channel forms of the magnetorheological fluid are annular channel and disc channel. The annular channel has a simple structure and convenient installation, and it can decrease the volume of the buffer effectively. As for the disc channel, although the structure is relatively complex, its special structure can improve the utilization rate of the magnetic field and buffer force. Therefore, the annular channel and disc channel are combined as a mixed channel in this paper. Figure 6 is the structure of the mixed channel; it not only ensures small volume of the buffer, but also improves the performance of the buffer by promoting the utilization rate of the magnetic field.

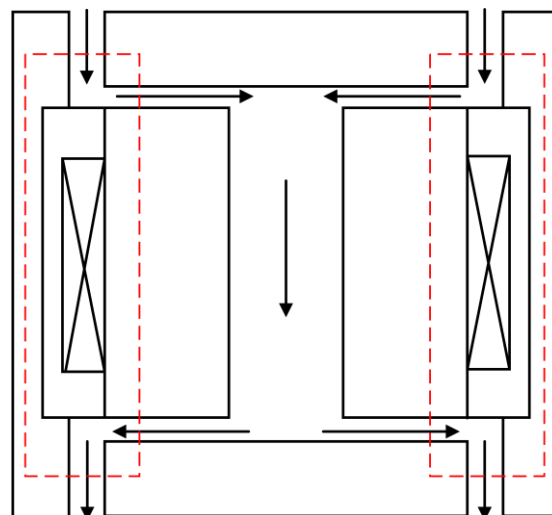


Figure 6. Mixed-channel structure.

3.1.2. Coil Number

As the input source of the buffer, the number of the electromagnetic coil has an important influence on the buffer performance. The coil has had single circle and multiple circles in recent research. A single circle is suitable for the magnetorheological buffer, which has a small volume; it can reduce control difficulty and improve space utilization. Although multiple circles have higher control difficulty, the diversity of the control strategies and the error-tolerant rate of the buffer are promoted. Because the VSB designed in this paper should have small volume and brief structure, the single circle is selected.

Coil turn is also a factor that has an effect on buffer force. In this paper, the coil turn is defined as the ratio of the area at the coil to the cross-sectional area of the single-turn coil. However, in the actual process of winding coil, a gap is generated between the coils, which leads to the actual turn number to be less than the calculated value. Thus, η is defined as a gap coefficient to eliminate the effect of the gap between coils on coil turn. The gap coefficient depends on coil diameter. The larger the wire diameter selected for the coil, the larger the gap and the greater η . After correction, the calculation formula of the coil turns is:

$$N = \eta \cdot \frac{CoilR \cdot CoilH}{S} \quad (1)$$

where N is coil turns, $CoilR$ is the groove depth at the coil, $CoilH$ is the groove width at the coil and the product of the two is the area at the coil. S is the cross-sectional area of wires. η is taken as 0.78 in this paper.

3.1.3. Combination of Damping Unit and Damping Cylinder

The combination modes of the damping unit and damping cylinder include embedded type and bypass type. Bypass type occupies a large volume, but it is more convenient to install and replace parts, and the piston neutral problem does not affect the buffer force. Embedded type is a piston with a coil moving in a sealed damping cylinder, changing the magnetic field of the magnetorheological fluid in the cylinder and squeezing the magnetorheological fluid to produce buffer force. An embedded buffer has a compact structure, small occupied volume and high magnetic field utilization, so the embedded scheme is selected as the combination of damping unit and damping cylinder in this paper.

3.2. Material Design

3.2.1. Magnetorheological Fluid

As the core material of magnetorheological buffer, the performance requirements of magnetorheological fluid mainly include low zero-field viscosity and high maximum shear yield strength. The viscosity of magnetorheological fluid increases and transforms into Bingham fluid in a very short time when it is affected by magnetic field, and it is a Newtonian fluid without a magnetic field. The typical Bingham model can be described as:

$$\begin{cases} \tau = \mu_0\gamma + \tau_y, & \tau > \tau_y \\ \gamma = 0, & \tau \leq \tau_y \end{cases} \quad (2)$$

where τ (Pa) is the shear stress of magnetorheological fluid. μ_0 (Pa·s) is the zero-field viscosity of magnetorheological fluid, an important parameter to measure the performance of magnetorheological fluid. τ_y (Pa) is the shear yield strength of the magnetorheological fluid. γ (s⁻¹) is the shear rate of the magnetorheological fluid, that is:

$$\gamma = \frac{du}{dy} \quad (3)$$

In the Bingham model, the magnetorheological fluid in the plug flow area is non-differentiable, which makes it difficult to solve in practical calculation. Therefore, through consulting the literature, this paper uses the approximate Bingham plastic model proposed

by David Case [18]. The model becomes continuously differentiable by decomposing the plug flow area into continuous tiny regions, which can be described as:

$$\tau = \left(\frac{\tau_y \tanh(\delta\gamma)}{\sqrt{\varepsilon^2 + \gamma^2}} + \mu_0 \right) \cdot \gamma \quad (4)$$

where ε is a constant used to eliminate discontinuities, usually approaching 0 in this model. δ is the proportional term of the slope, usually approaching infinity. The dynamic viscosity of the magnetorheological fluid obtained by deformation of Equation (4) is:

$$\mu = \frac{\tau_y \tanh(\delta\gamma)}{\sqrt{\varepsilon^2 + \gamma^2}} + \mu_0 \quad (5)$$

MRF-122EG magnetorheological fluid produced by the American LORD Company is adopted in this paper. Its specific performance parameters are shown in Table 1.

Table 1. MRF-122EG performance parameters.

Parameter	Value	Unit
Density	2.28~2.48	g/cm ³
Zero-field viscosity	0.042	Pa·s
Mass fraction	72.00	%
Temperature	−40~130	°C
Color	Black gray	

In order to couple the electromagnetic field with the flow field, the relationship between the yield stress τ (kPa) and the magnetic induction B (T) of MRF-122EG is obtained by curve fitting:

$$\tau = 89.26B^4 - 237.1B^3 + 165.6B^2 + 17.22B - 0.31 \quad (6)$$

3.2.2. Valve Core Material

Valve core material is soft magnetic material that is prone to magnetization and demagnetization processes and has low coercive force. Industrial pure iron is one of the most widely used soft magnetic materials [19]; the performance of saturation magnetic induction and magnetic permeability in soft magnetic materials is excellent, but high conductivity also leads to high loss. Soft magnetic materials affect the response time of magnetorheological buffers through conductivity. According to the current research status of soft magnetic materials, new composite material has a large magnetic saturation induction intensity, so it does not reach the magnetic saturation in practical application and does not affect the maximum buffer force. Therefore, in order to improve the dynamic response velocity of the buffer, this paper chooses new composite material as the soft magnetic material of the valve core.

3.2.3. Cylinder Material

The cylinder body is one of the most important parts of the magnetic circuit of magnetorheological buffers; its magnetic property plays a key role in the magnetic performance. As for the selection of cylinder material, on the one hand, the material should have good magnetic properties. On the other hand, due to the diameter of the designed buffer being very small, the cylinder material should have better processing performance, which has the ability to maintain strength while being machined to a small diameter and small thickness. At present, the most widely used cylinder material is industrial pure iron, which has good magnetic properties but is not easy to process. Therefore, this paper chooses No. 10 steel as the cylinder material of the buffer, which has similar magnetic properties to industrial pure iron but has better machinability and lower price.

3.3. Dimension Design

After selecting the mixed-channel, embedded VSB structure scheme, the key dimensions need to be structurally designed; the structure of the design buffer is shown in Figure 7. The buffer is connected to the magnetic disk and the valve core is moved up and down by a piston rod. The magnetorheological fluid flows in the mixed channel. After the coil is energized, the magnetorheological effect occurs, so the viscosity of the magnetorheological fluid increases and outputs the controllable buffer force. According to the design requirements, the designed buffer can output buffer force of about 100 N with a maximum current of 2.5 A and a damping unit velocity of 0.5 m/s. The selected design variables and their ranges are shown in Table 2.

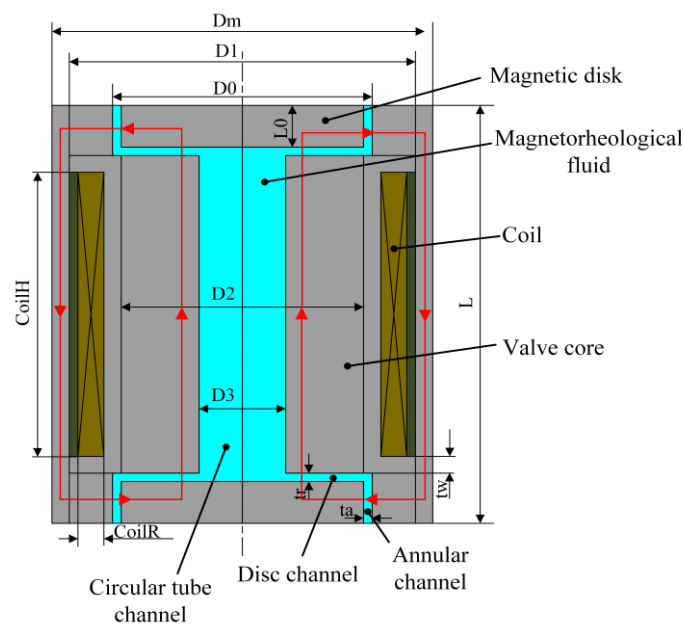


Figure 7. Structure parameters of the VSB.

Table 2. The range of designed variables for the VSB.

Variable	Physical Meaning	Range (mm)
D2	Outer diameter of spool	3~6
D3	Diameter of circular tube channel	1~3
ta	Gap of annular channel	0.1~0.3
tr	Gap of disc channel	0.5~2
CoilR	Depth of coil slot	0.5~2
CoilH	Width of coil slot	30~35

3.4. Optimization Design

At present, the most commonly used optimization algorithms in structural optimization include the multi-objective optimization algorithm [20], bound optimization BY quadratic approximation (BOBYQA) algorithm [21], Nelder–Mead (N-M) algorithm [22–24] and so on. In the actual optimization process, different optimization objectives cannot achieve the optimal value at the same time. Both BOBYQA and N-M optimize targets based on established finite element models. The optimization object of this paper is the buffer, and the optimization parameter is the dimension parameter of the buffer. The adjustable coefficient of buffer force is taken as the objective function of optimization, which is single-objective optimization. The ultimate goal is to make the adjustable coefficient of the buffer reach the maximum value. Because the modeling software used in this paper and the co-simulation platform COMSOL Multiphysics have a built-in N-M algorithm, the

optimization can be directly processed after modeling, which can greatly improve efficiency and save time. Therefore, this paper uses the N-M algorithm to optimize the dimension of the buffer. The workflow of the N-M algorithm is shown in Figure 8.

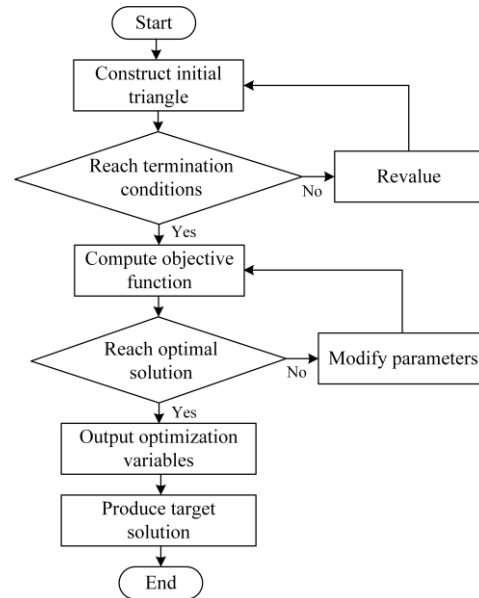


Figure 8. Workflow of N-M optimization algorithm.

1. Build an initial triangle based on the given data points. The best point $x_1^{(k)}$ is B (Best); the other two points $x_2^{(k)}$ and $x_3^{(k)}$ are G (Good) and W (Worse), respectively; k is current iteration times;
2. Generate point $x_r^{(k)}$ by reflecting the W (Worse):

$$x_r^{(k)} = \bar{x}^{(k)} + \alpha (\bar{x}^{(k)} - x_3^{(k)}) \quad (7)$$

where α is reflection coefficient, usually taken as 1. $\bar{x}^{(k)}$ is the center of figure:

$$\bar{x}^{(k)} = \frac{1}{n} \sum_{i=1}^n x_i^{(k)} \quad (8)$$

In two-dimensional space, n is 2. If $f(x_1^{(k)}) \leq f(x_r^{(k)}) \leq f(x_3^{(k)})$, the direction of reflection is correct to the target value, then the iteration is terminated. If $f(x_1^{(k)}) > f(x_r^{(k)})$, turn to the third step. Otherwise, take the fourth step;

3. Construct expansion point $x_e^{(k)}$ in the same direction of the reflection point:

$$x_e^{(k)} = \bar{x}^{(k)} + \beta (\bar{x}^{(k)} - x_r^{(k)}) \quad (9)$$

where β is the expansion coefficient, usually taken as 2. If $f(x_e^{(k)}) < f(x_r^{(k)})$, replace $x_3^{(k)}$ with $x_e^{(k)}$ and terminate iteration. Otherwise, replace $x_3^{(k)}$ with $x_r^{(k)}$ and terminate iteration;

4. Choose shrinkage mode. If $f(x_2^{(k)}) \leq f(x_r^{(k)}) \leq f(x_3^{(k)})$, point $x_c^{(k)}$ is generated:

$$x_c^{(k)} = \bar{x}^{(k)} + \gamma (x_r^{(k)} - \bar{x}^{(k)}) \quad (10)$$

where γ is shrinkage coefficient, usually taken as 0.5. If $f(x_c^{(k)}) \leq f(x_r^{(k)})$, replace $x_3^{(k)}$ with $x_c^{(k)}$ and terminate iteration. Otherwise, take the fifth step.

If $f(x_r^{(k)}) \geq f(x_3^{(k)})$, iterate to obtain the point $x_{cc}^{(k)}$:

$$x_{cc}^{(k)} = \bar{x}^{(k)} - \gamma (x_r^{(k)} - \bar{x}^{(k)}) \quad (11)$$

If $f(x_{cc}^{(k)}) < f(x_3^{(k)})$, replace $x_3^{(k)}$ with $x_{cc}^{(k)}$ and terminate iteration. Otherwise, take the fifth step;

5. Shrink point:

$$x_i^{(k+1)} = x_1^{(k)} + \delta (x_i^{(k)} - x_1^{(k)}) \quad (12)$$

where the range of shrinkage coefficient δ is 0~1, usually taken as 0.5, $\forall i \in \{2, \dots, n + 1\}$. Repeat steps 1 to 5 until the termination condition of the iteration is reached or the maximum number of iterations is reached. The final approximate solution of the unknown target value x is represented by the optimal solution \hat{x} .

According to the above-selected objective function, optimization variables and optimization algorithm, the multi-physics finite element model of the designed buffer is established, and the relevant settings are carried out in COMSOL software. It is found that the adjustable coefficient reaches a stable value of about 24.76 after about 280 iterations. The optimized variables and the rest key parameters of the buffer are shown in Table 3.

Table 3. Main structure parameters of the buffer after optimization.

Optimization Variable	Value (mm)	Rest Parameter	Value (mm)
D2	4	Dm	8.5
D3	1.25	D0	4.5
ta	0.25	D1	7.5
tr	1	tw	2
CoilR	1	L	50
CoilH	34	L0	5

The diameter of the optimized buffer is negligibly small, and the space of coil is small, so it is necessary to select the diameter of the copper winding to be as small as possible when the maximum current is 2.5 A. By querying the related information of varnished wire, the varnished wire of type QY-2/2200.100GB6109.6-88 is selected. According to the optimized structural parameters and Equation (1), the coil turns of the designed buffer are 136, and the optimized coil has two radial winding layers and 63 axial winding laps.

4. Simulation and Analysis

4.1. Simulation of the Designed VSB

Through the above design and dimension optimization of the VSB, the 3D structure of the designed buffer is as shown in Figure 9. Meanwhile, the geometric model and the magnetic field distribution of the designed VSB are as shown in Figure 10. The left side is the established 2D axisymmetric geometric model of the buffer, and the right side is the distribution of its magnetic field. It can be seen that the magnetic induction line of the buffer is evenly distributed, showing a symmetrical shape relative to the midpoint of the valve core, and the maximum value of the magnetic induction intensity appears at the place of valve core. Above all, the magnetic circuit and structural design of the buffer are reasonable.

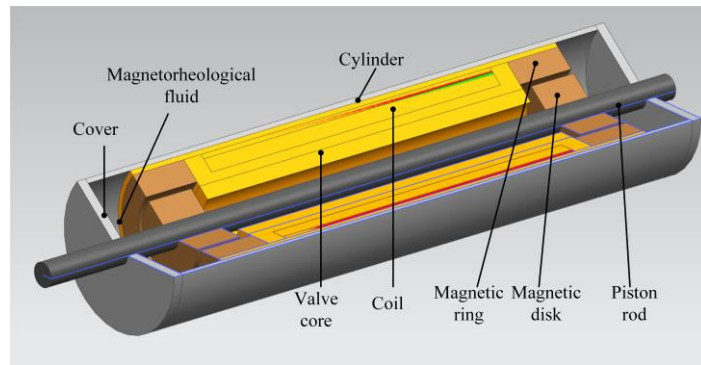


Figure 9. 3D structure of the designed VSB.

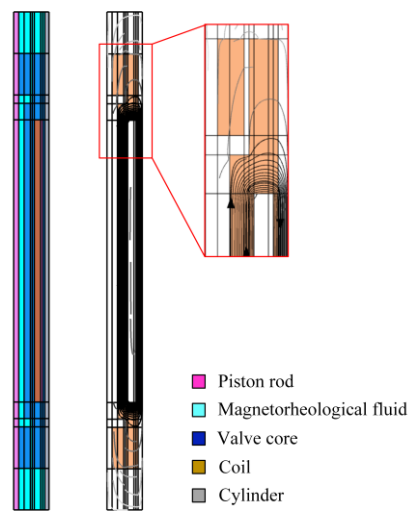


Figure 10. Geometric model and the magnetic field distribution of the designed VSB.

After establishing the multi-physics finite element model of the buffer, it is solved statically. When the current of coil is 2.5 A, the motion curve of the damping unit is a sine curve with an amplitude of 4 mm and a period of 0.05 s; the relationship between the output buffer force and the piston displacement is shown in Figure 11, and the relationship between the output buffer force and the velocity is shown in Figure 12. It can be seen that the output buffer force is positively correlated with the velocity of the piston and the current of the coil. The buffer force is 3.4 N when the coil does not have applied current, and the adjustable coefficient is 24.76. When the maximum input current is 2.5 A, the maximum buffer force reaches 84.2 N.

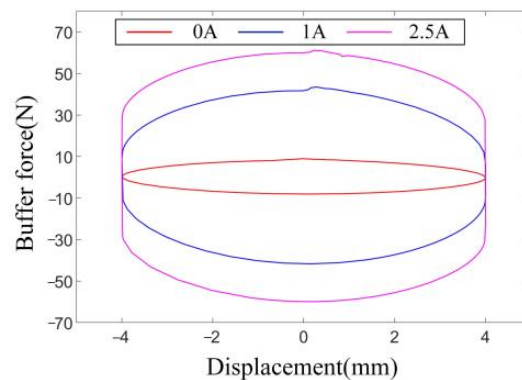


Figure 11. Curve between buffer force and displacement of the VSB.

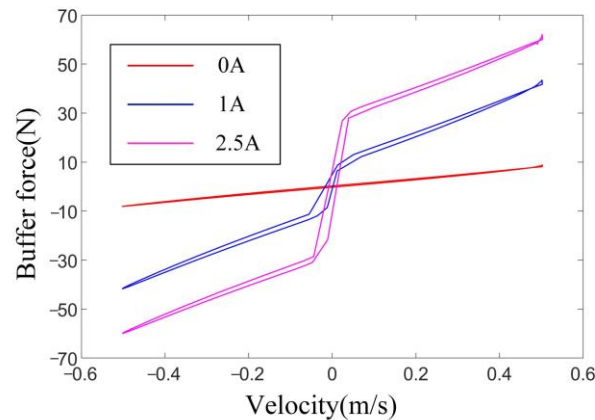


Figure 12. Curve between buffer force and velocity of the VSB.

In order to improve the response time of the designed buffer, transient simulation is needed. The stable current of the coil is set to 2.5 A, and the moving velocity of the damping unit is 0.1 m/s. The response time of the buffer force is shown in Figure 13. As can be seen from the figure, after optimizing the buffer dimension parameters, not only does the buffer force have a significant increase, but also the response time is improved from 9 ms to 1.3 ms. It is indicated that the work of structural optimization provides omni-bearing promotion for the overall performance of the buffer.

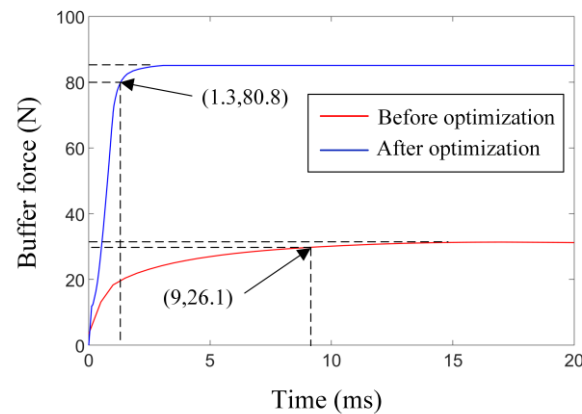


Figure 13. Buffer force curves of the designed VSB.

4.2. Construction of Co-Simulation Platform

In this paper, the coupling relationship of the designed EMVV system is studied, and a co-simulation platform is built to lay the foundation for studying the valve seating performance. At the macro level of the entire system, the EMVA and VSB have a complex coupling relationships, as shown in Figure 14. It can be seen that, in addition to the coupling relationship between the actuator and the buffer, they are also coupled to each other by the buffer force and the velocity of the coil. The buffer force output by the buffer and the electromagnetic force generated by the actuator are added together to drive the coil, and the velocity of the coil is also the input condition of the buffer for the piston motion.

The default data transfer channel between COMSOL and MATLAB/Simulink can realize the function of real-time data transmission. The latest version of COMSOL implements real-time transmission between the data and command by COMSOL Multiphysics with Simulink. Based on the data channel, the steps of building the co-simulation are:

1. Build the finite element models of the actuator and the buffer in COMSOL;
2. Set the input and the output of the actuator and the buffer in COMSOL. The input of the actuator is the voltage of the coil and the buffer force, and the output is the velocity and the displacement of the coil. The input of the buffer is the voltage of the

- coil and the velocity of the piston, and the output is the buffer force. Then, save the finite element models as .slx files, recognizable by MATLAB/Simulink;
3. Import the .slx files of the actuator and the buffer to MATLAB/Simulink. Build the co-simulation model based on the coupling relationship between the actuator and the buffer;
4. Set the input and the output of the system and set calculation time and time step;
5. Solve to obtain the calculation results.

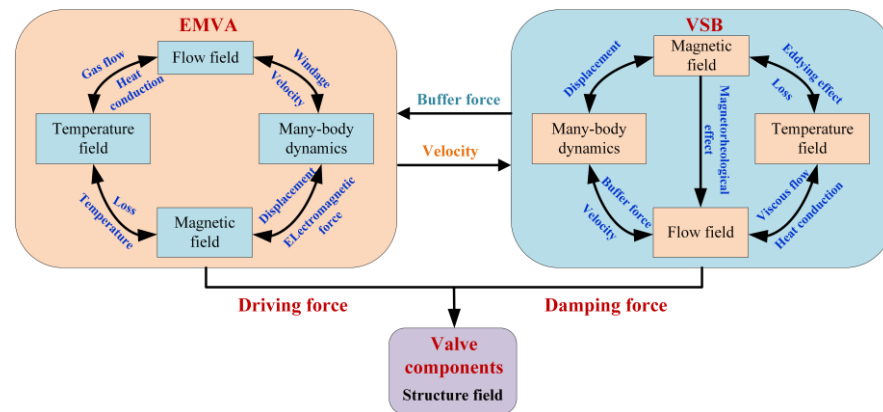


Figure 14. Coupling relationship of EMVV system.

The co-simulation of the EMVV system is carried out based on the above steps. Figure 15 is the co-simulation model of the entire system. After building the model, it is necessary to set the input voltage of the actuator and the buffer and adjust the computing time and step in MATLAB/Simulink. The solution process of the whole co-simulation is carried out in COMSOL. After each step of calculation, the data are transmitted to MATLAB/Simulink in real time, then the calculation is carried out according to the coupling relationship of the model. Finally, the calculated data are post-processed in MATLAB.

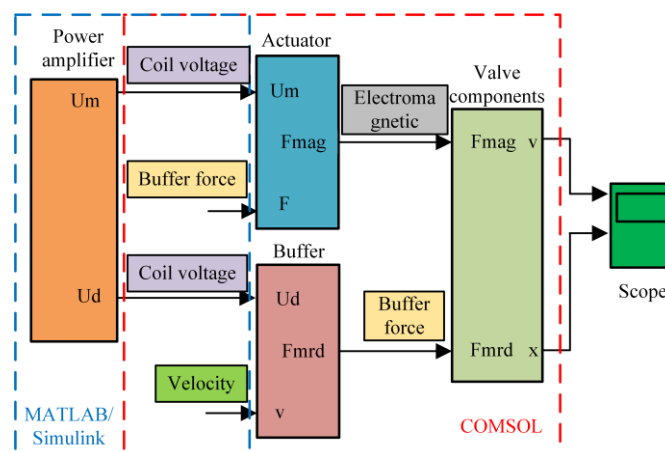


Figure 15. Co-simulation model of EMVV system.

4.3. Analysis of Valve Seating Performance

The electromagnetic valve seating is simulated under specific conditions based on the established co-simulation platform. The EMVA applies a sinusoidal current with an amplitude of 10 A and a frequency of 5 Hz, where the valve is at the top at the beginning of the simulation. The input excitation of the buffer is a pulse current with an amplitude of 0.5 A, a frequency of 10 Hz and a duty cycle of 5%, which ensures that the buffer can output stable buffer force during the period from the valve seating to the valve stability. In the meantime, through the dynamic analysis of the buffer, its response time is 1.3 ms,

so opening the buffer 1.5 ms before valve seating is enough to make the buffer output a constant buffer force to reduce the valve seating velocity. The simulation results are shown in Figure 16. The lift of the valve is 8 mm. Before and after the opening of the buffer, the valve seating velocity decreases from 0.58 m/s to 0.03 m/s, and the valve rebound height decreases from 0.67 mm to 0.02 mm. Therefore, it is indicated that the design buffer can obviously reduce the seating velocity and the rebound height of the valve and achieve good valve seating performance.

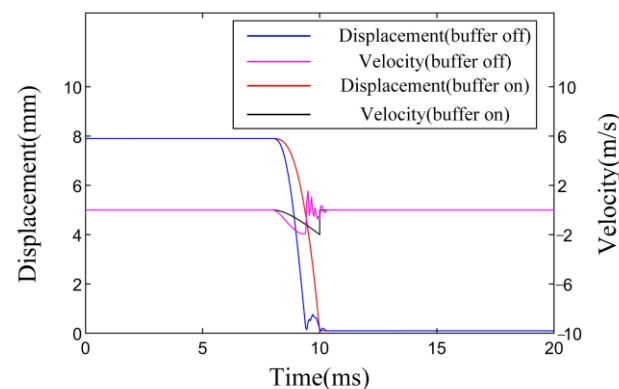


Figure 16. Co-simulation results of EMVV system.

5. Conclusions

In this paper, an external buffer is proposed, aiming to resolve the problem of large impact and noise of EMVV landing. The structure, material and dimension design process of the VSB rdescribed in detail, and the key size parameters of the buffer are optimized based on the N-M algorithm. Meanwhile, the coupling relationship between the actuator and the buffer in the EMVV system is studied; a scheme where the VSB is embedded in the EMVA is proposed. In addition, a COMSOL and MATLAB/Simulink co-simulation platform and co-simulation model are built based on the scheme. Finally, the results of the co-simulation are compared, and the valve seating performance is analyzed.

The integration scheme proposed in this paper not only improves the integration of the system, but also greatly reduces the volume of the whole system, which is a tremendous boost for the engine in its limited setting space. Furthermore, the valve seating velocity and the valve rebound height are reduced from 0.58 m/s and 0.67 mm to 0.03 m/s and 0.02 mm, and the reduction ratios are 94.8% and 97%, respectively. The co-simulation results show that opening the designed buffer before the valve seating can obviously relieve the valve seating impact, overwhelmingly improve the valve seating performance of the EMVV system and prolong the engine life. However, due to the small radial dimension of the designed buffer, machining accuracy and assembling mode are strongly required in processing. Therefore, it is necessary to further optimize the combination of the damping unit and the damping cylinder and the assembling mode of the damping unit of the buffer.

Author Contributions: Conceptualization, methodology, software, validation and formal analysis, Q.Z., L.L. and C.Z.; investigation, Q.Z., L.L., Z.X. and X.W.; data curation, Q.Z. and C.Z.; writing—original draft preparation, Q.Z. and L.L.; writing—review and editing, Q.Z. and L.L. All authors have read and agreed to the published version of the manuscript.

Funding: This work was funded by the National Natural Science Foundation of China, grant numbers 51975297 and 51875290.

Data Availability Statement: Not applicable.

Conflicts of Interest: The authors declare no conflict of interest.

References

1. Kuruppu, C.; Pesiridis, A.; Rajoo, S. *Investigation of Cylinder Deactivation and Variable Valve Actuation on Gasoline Engine Performance*; SAE World Congress and Exhibition: Detroit, MI, USA, 2014; pp. 7484–7492.
2. Reinholz, B.A.; Reinholz, L.; Seethaler, R.J. Optimal trajectory operation of a cogging torque assisted motor driven valve actuator for internal combustion engines. *Mechatronics* **2018**, *51*, 1–7. [[CrossRef](#)]
3. Fan, X.; Yin, J.; Lu, Q. Design and analysis of a novel composited electromagnetic linear actuator. *Actuators* **2022**, *11*, 6. [[CrossRef](#)]
4. Yang, Y.; Liu, J.; Ye, D.; Chen, Y.; Lu, P. Multiobjective optimal design and soft landing control of an electromagnetic valve actuator for a camless engine. *IEEE-ASME Trans. Mechatron.* **2013**, *18*, 963–972. [[CrossRef](#)]
5. Paden, B.A.; Snyder, S.T.; Paden, B.E.; Ricci, M.R. Modeling and control of an electromagnetic variable valve actuation system. *IEEE-ASME Trans. Mechatron.* **2015**, *20*, 2654–2665. [[CrossRef](#)]
6. Tu, B.; Tian, H.; Wei, H.; Pan, M. Research on buffering process of electro-hydraulic variable valve train. *China Mech. Eng.* **2016**, *27*, 2652. [[CrossRef](#)]
7. Pan, K.; Wang, Z.; Tian, F.; Chen, J. Simulation study on the buffering process of valve seating buffer mechanism. *Mod. Mach.* **2016**, *2*, 47–49. [[CrossRef](#)]
8. Xu, R.; Chang, S. Dynamic analysis and buffer structure for electromagnetic valve actuation. *Veh. Engine* **2015**, *06*, 8–12. [[CrossRef](#)]
9. Case, D.; Taheri, B.; Richer, E. Multiphysics modeling of magnetorheological dampers. *Int. J. Multiphys.* **2013**, *7*, 61–76. [[CrossRef](#)]
10. Gurubasavaraju, T.M.; Kumar, H.; Mahalingam, A. An approach for characterizing twin-tube shear-mode magnetorheological damper through coupled FE and CFD analysis. *J. Braz. Soc. Mech. Sci. Eng.* **2018**, *40*, 139. [[CrossRef](#)]
11. Alan, S.; René, Z.; Juan, C. Multiphysics behavior of a magneto-rheological damper and experimental validation. *Eng. Struct.* **2014**, *15*, 194–205.
12. Mao, M.; Choi, Y.T.; Wereley, N.M. Effective design strategy for a magnetorheological damper using a nonlinear flow model. In Proceedings of the Smart Structures and Materials 2005 Conference, San Diego, CA, USA, 7–10 March 2005; pp. 446–455.
13. Guan, X.; Guo, P.; Ou, J. Multi-objective optimization of magnetorheological fluid dampers. *Eng. Mech.* **2009**, *26*, 30–35.
14. Wu, J.; Wang, H. Magnetic circuit optimum design of a magneto-rheological damper based on ANSYS. *Mech. Electr. Eng. Mag.* **2008**, *25*, 74–76. [[CrossRef](#)]
15. Yang, X.; Chen, Y.; Liu, Y.; Zhang, R. Modeling and experiment of an annular multi-channel magnetorheological valve. *Actuators* **2022**, *11*, 19. [[CrossRef](#)]
16. Zheng, C.; Liu, L.; Guo, H.; Xu, Z. Optimization design of a fully variable valve system based on Nelder-Mead algorithm. *Proc. Inst. Mech. Eng. Part C-J. Mech. Eng. Sci.* **2022**, *236*, 5815–5825. [[CrossRef](#)]
17. Sheng, L.; Liu, J.; Yu, Z. Dynamic modeling of a flexible multi-body system with elastic impact. *J. Shanghai Jiaotong Univ.* **2006**, *40*, 1790–1793. [[CrossRef](#)]
18. Case, D.; Taheri, B.; Richer, E. Dynamical modeling and experimental study of a small scale magnetorheological damper. *IEEE-ASME Trans. Mechatron.* **2014**, *19*, 1015–1024. [[CrossRef](#)]
19. Li, Z.; Dong, Y.; Pauly, S.; Chang, C.; Wei, R.; Li, F.; Wang, X. Enhanced soft magnetic properties of Fe-based amorphous powder cores by longitude magnetic field annealing. *J. Alloys Compd.* **2017**, *706*, 1–6. [[CrossRef](#)]
20. Cha, Y.; Agrawal, A.K.; Phillips, B.M.; Spencer, B.F. Direct performance-based design with 200 kN MR dampers using multi-objective cost effective optimization for steel MRFs. *Eng. Struct.* **2014**, *71*, 60–72. [[CrossRef](#)]
21. Zheng, J.; Li, Y.; Wang, J. Design and multi-physics optimization of a novel magnetorheological damper with a variable resistance gap. *Proc. Inst. Mech. Eng. Part C-J. Mech. Eng. Sci.* **2017**, *231*, 3152–3168. [[CrossRef](#)]
22. Fakhouri, H.N.; Hudaib, A.; Sleit, A. Hybrid particle swarm optimization with sine cosine algorithm and Nelder–Mead simplex for solving engineering design problems. *Arab. J. Sci. Eng.* **2020**, *45*, 3091–3109. [[CrossRef](#)]
23. Zic, M.; Pereverzyev, S. Optimizing noisy CNLS problems by using Nelder-Mead algorithm: A new method to compute simplex step efficiency. *J. Electroanal. Chem.* **2019**, *851*, 113439. [[CrossRef](#)]
24. Abdelrahman, E.M.; Abdelazeem, M.; Gobashy, M. A minimization approach to depth and shape determination of mineralized zones from potential field data using the Nelder-Mead simplex algorithm. *Ore Geol. Rev.* **2019**, *114*, 103123. [[CrossRef](#)]

Disclaimer/Publisher’s Note: The statements, opinions and data contained in all publications are solely those of the individual author(s) and contributor(s) and not of MDPI and/or the editor(s). MDPI and/or the editor(s) disclaim responsibility for any injury to people or property resulting from any ideas, methods, instructions or products referred to in the content.